Journal of Alloys and Compounds 684 (2016) 481–487

Contents lists available at ScienceDirect

Journal of Alloys and Compounds

journal homepage: http://www.elsevier.com/locate/jalcom

Solute clustering behavior between 293K and 373K in a 6082 Aluminum alloy

V. Noseda Grau [a, c, *], A. Cuniberti [a, c], A. Tolley [b, c], V. Castro Riglos [b, c], M. Stipcich [a, c]

[a] Instituto de Física de Materiales Tandil – IFIMAT, Facultad de Ciencias Exactas, Universidad Nacional del Centro de la Provincia de Buenos Aires, Pinto 399, 7000, Tandil, Argentina
[b] Centro Atómico Bariloche, Comisión Nacional de Energía Atómica, Av. Bustillo 9500, 8400, San Carlos de Bariloche, Argentina
[c] Consejo Nacional de Investigaciones Científicas y Técnicas (CONICET), Argentina

ARTICLE INFO

Article history:
Received 26 February 2016
Received in revised form
2 May 2016
Accepted 18 May 2016
Available online 20 May 2016

Keywords:
Al–Mg–Si alloy
Clustering
DSC analysis
Hardness
Transmission electron microscopy

ABSTRACT

We present a systematic study of the effect of pre-ageing between 293 K and 373 K in a 6082 Aluminum alloy using mainly differential scanning calorimetry in combination with Vickers hardness and transmission electron microscopy. The pre-ageing effects are characterized through the modifications of the β″ precipitation DSC signal. Pre-ageing at 293 K leads to a progressive increase of the peak temperature, until it reaches a plateau at long aging times (≥250min), while pre-ageing at 373 K leads to a continuous decrease of the peak temperature. The results indicate the formation of two different types of clusters, named 1 and 2, below and above a pre-ageing transition temperature, determined to be around 343 K. After pre-ageing below 343 K, the dissolution of clusters 1 superimposed with the β″ precipitation occurs, and the enthalpy change remains almost independent of pre-ageing time. Instead, pre-ageing above 343 K leads to the formation of type 2 clusters that transform on heating into β″ phase precipitates, with a decreasing enthalpy change as pre-ageing time increases. This result indicates that clusters 2 evolve during pre-ageing, reaching a structure/composition with formation enthalpy similar to that of β″ phase. Vickers hardness reveals the different evolution of both types of clusters with aging time. Transmission electron microscopy observations on samples subsequently aged at 453 K, show that type 2 clusters favour the nucleation of β″ precipitates, while type 1 clusters hamper such nucleation process.

1. Introduction

Al–Mg–Si alloys are being increasingly applied in a wide range of engineering applications, mainly in transportation and building. In these alloys an extremely rich variety of solute aggregation states have been observed, including solute clustering and different metastable phases, depending on the alloy composition, temperature and ageing time. The precipitation sequence has been investigated by many researchers and can be schematically presented as [1,2]:

SSS → Mg/Si clusters → Guinier Preston zones → β″ precipitates → β′ precipitates → β phase

where SSS is the supersaturated solid solution, β phase is the equilibrium Mg_2Si phase [3], and in between a series of metastable solute rich configurations have been reported [4–6]. Such sequence is not valid for every temperature, since some of the phases might not occur at low or high temperature, or may transform into others at high temperature [7–10]. There also may be temperature ranges

* Corresponding author. IFIMAT – UNICEN, Pinto 399, 7000, Tandil, Argentina.
E-mail address: vnosedagrau@gmail.com (V. Noseda Grau).

http://dx.doi.org/10.1016/j.jallcom.2016.05.197
0925-8388/

of co-existence of more than one phase [9–11]. Ageing at low temperature, between 273 K and 373 K, leads to different kind of Mg and Si clustering. The excess amount of solute atoms that are homogeneously distributed in the matrix just after quenching, SSS condition, establish a high energy condition. Due to its difference in size and/or in electron affinity relative to the Al atoms, each solute atom will strain the matrix locally [12]. When Mg and Si are combined, they compensate for their large and small atomic size, causing less strain in the surrounding Al lattice. This means that supersaturation already constitutes a strong driving force toward solute clustering. Eventual energetically favorable chemical bonding can set up additional driving forces toward nucleation, of which the Mg–Si bond is the strongest [13]. Because they are highly coherent with the matrix [7,14], clusters have a very low interfacial energy. Additionally there is very little misfit strain, minimizing the activation energy barrier for their formation.

The formation of clusters during aging at 293 K (natural aging, NA) has been widely studied [15–20], because such clusters reduce the nucleation rate of β″ phase, and consequently produce a slow hardening response of the material under artificial aging (AA) [7,9,14,21–25]. The formation of clusters at slightly higher temperatures has been less examined. However, cluster formation during ageing at temperatures in the range 343 K–373 K has been addressed [8,14,16,26–30], and there is good agreement that these clusters are nuclei of the β″ phase. Despite the vast amount of reported information, most of the studies were performed after aging at a fixed temperature and aging time. All the clusters are extremely small, just a few nanometers in size, fully coherent with the matrix and do not have a distinct structure [7,14]. The best technique to analyze nanoscale clusters is 3D atom probe. However, transmission electron microscopy (TEM), and other indirect techniques such as thermal analysis, mechanical testing, X-ray scattering and positron annihilation spectroscopy, are able to contribute significant information.

The aim of this work is to present a systematical study of the clusters formed in the temperature range between 293 K and 373 K, and their evolution with ageing time. We use differential scanning calorimetry (DSC) to follow the clusters' effects on the subsequent precipitation of the β″ phase, complemented with Vickers hardness (Hv), and transmission electron microscopy (TEM). DSC provides unique quantitative information about the relative stability and formation enthalpy of metastable phases. Moreover, DSC plus hardness measurements provide a comprehensive picture of the clusters' evolution.

2. Experimental

The alloy under study was a commercial AW-6082 alloy (Alcoa Europe) with nominal composition Al–1.07-Si–0.72Mg–0.61Mn–0.04Cu–0.21Fe (wt%), received in form of hot-rolled 10 mm thick sheet. The relation Mg_2Si is ≈ 1.1 wt%, with 0.6 wt% Si excess. Samples for DSC were prepared as disks with 4.5 mm diameter and 2 mm thickness. Samples for Hv determinations were prepared as plates with around $(10 \times 20)mm^2$ area and 1.5 mm thickness. Before testing, the samples were solution-treated at 823 K for 30 min, and subsequently quenched into room temperature (RT) water. Pre-ageing (PA) thermal treatments between 293 K and 373 K were performed in two ways, both with PID temperature control. DSC disks were annealed in a thermal bath. The Hv samples were annealed between heating plates. The temperature was monitored with a K-type thermocouple welded to a reference sample, recording the temperature-time data with a data logger. The PA temperature variation was less than ±2 K. The DSC tests were conducted with a Rheometric Scientific DSC SP calorimeter. The Hv determinations were conducted with a Mitutoyo indenter using a 100 g load. TEM observations were carried out using a Tecnai F20 microscope. For TEM observations, 3 mm diameter discs were cut by spark erosion from the plates for hardness measurement, and their thickness was reduced to about 150 μm by mechanical grinding, Final thinning was carried out with double jet electropolishing, as described elsewhere [22].

3. Results

3.1. DSC analysis and hardness measurements

Fig. 1 contains representative DSC thermograms obtained in samples with increasing PA time at 293 K, 333 K, 353 K and 373 K. Two prominent exothermic peaks can be observed between 473 K and 523 K, identified as I and II, which correspond to the precipitation of the β″ and β′ phases, respectively [23,25,31,32]. It is worthy to note that no peaks are observed below 450 K as those reported in Refs. [16,27,29,31]. Since the analysis will focus mainly on the β″ phase precipitation, corresponding to peak I, a limited temperature range, 400 K–700 K, is shown. The following general features can be noted:

1) A temperature shift of peak I is observed in the thermograms as the PA time increases.
2) The area under peaks I do not change significantly when PA occurs at RT, while significant changes occur for PA at higher temperatures.
3) When PA is carried out at room temperature, a small endothermic peak around 483 K is observed, more pronounced as the NA increases. This endothermic peak is not observed when PA is carried out at higher temperatures.

In order to analyze in detail the temperature shifts of peak I, the peak temperature (Tp), that of maximum reaction rate $d^2Q/dT^2 = 0$, was selected as a characteristic parameter, since it can be determined with high precision. Indeed, differences below ±1 K in Tp were measured when DSC runs were repeated in each PA condition. Fig. 2 shows the evolution of Tp as a function of PA time and temperature. Pre-ageing at 293 K leads to an increase of Tp, until it reaches a plateau for t_{PA} longer that ≈250min. In contrast, the pre-aging at 373 K leads to a continuous decrease of Tp. Analysis of the data presented in Fig. 2 indicates that there is a transition temperature, somewhere in between 333 K and 353 K, above which the peak temperature increases with PA time and below which the opposite behavior occurs.

The heat associated to the β″ precipitation, Q, was measured as the integral area of the exothermic signal I, A_I. This released heat represents the enthalpy change (ΔH) associated with the precipitation reaction, where $\Delta H = Q = -A_I$. Fig. 3 presents the ΔH values against the PA time at 293 K and 373 K. The area corresponding to signal I in the thermograms of samples with PA at 293 K is difficult to determine due to the overlap of the exothermal signal of the precipitation of the β″ phase and the preceding endothermic signal, resulting in a large uncertainty. However, the results show that ΔH is almost constant as a function of pre-ageing time at 293 K. Instead, the enthalpy difference decreases progressively as pre-ageing time at 373 K increases, reaching a value of zero for PA of around 1400 min and longer.

In Fig. 4, the hardness evolution during isothermal aging at 373 K is compared with that during NA and AA at 453 K. A significant difference in the hardness evolution can be observed between aging at 293 K and 373 K. While Hv increases gradually with ageing time during NA, reaching a saturation value of 96 MPa after around 10^4 min (7 days), aging at 373 K leads to a slower increase of Hv up to about 1000 min, followed by a faster increase up to a value of

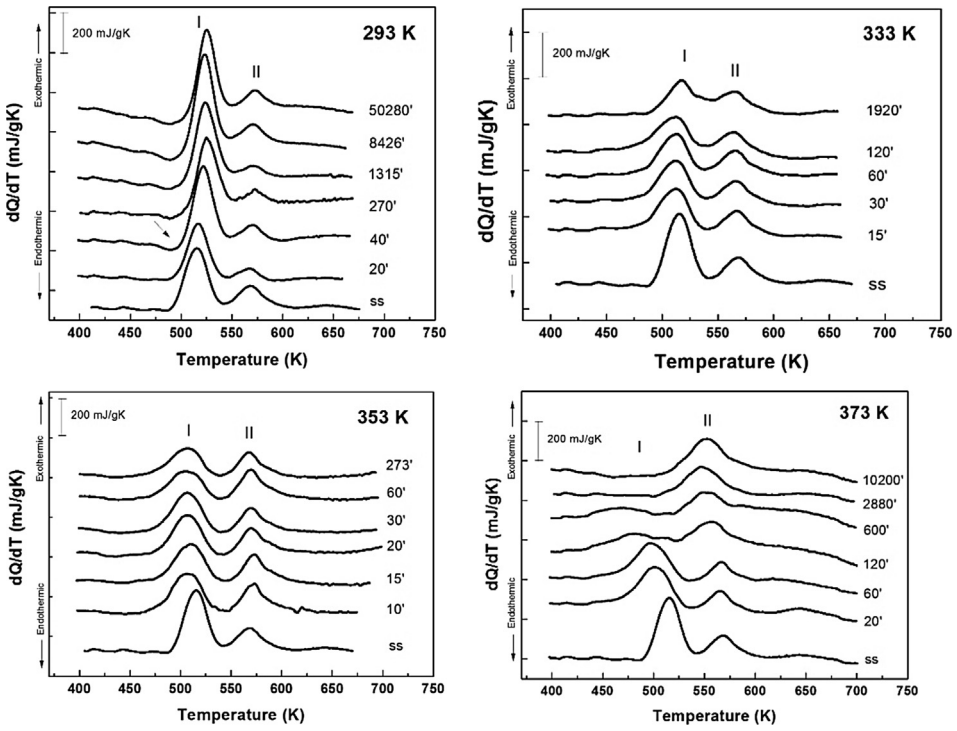

Fig. 1. Evolution of DSC thermograms with increasing pre-ageing time (in minutes) at different pre-ageing temperatures: 293 K, 333 K, 353 K, 373 K.

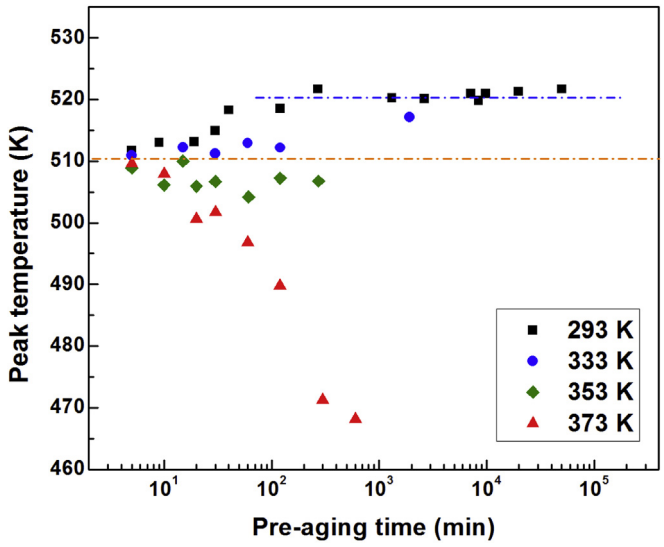

Fig. 2. Evolution of Tp, the peak temperature of peak I, with pre-ageing time at the different pre-ageing temperatures.

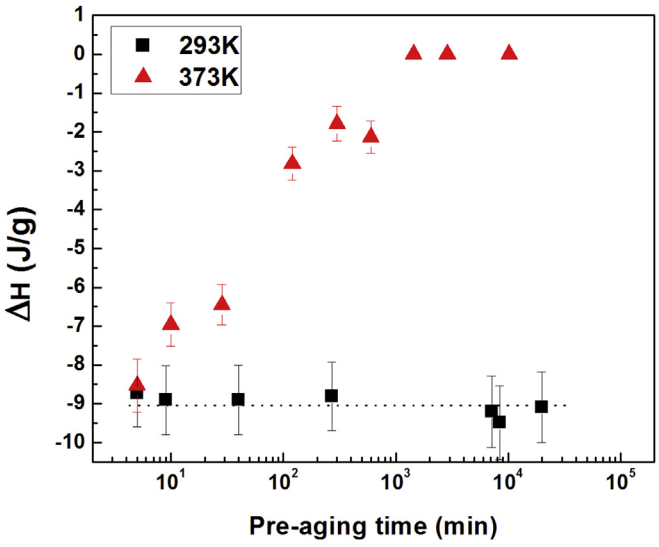

Fig. 3. Evolution of the enthalpy change associated with the precipitation of the β″ phase with pre-ageing at 293 K and 373 K.

133 MPa at about $5.9 \cdot 10^4$ min (≈40 days).

Fig. 5 compares the hardness evolution at 453 K after pre-ageing for 180 min at RT and 373 K. The hardness measured directly after solution treatment and quenching (SS) is shown for comparison. After RT pre-ageing, the hardness evolution shows an initial stage with a very slow hardness increase up to an ageing time of about 30 min, and then a second stage with a rapid hardness increase, reaching the peak ageing after about 120 min. Instead, after pre-ageing at 373 K, the fast hardness increase is shifted to shorter times, beginning after only 10 min of ageing. After about 30 min, hardness continues to grow at a lower rate, reaching the peak hardness at the same time as for RT pre-ageing, and with a similar value. Hardening after PA remains lower than that obtained under AA from the SS.

3.2. TEM characterization

Fig. 6 shows a TEM image of a sample aged one week (10^4min) at 373 K. A high density of small dark spots is observed, that is attributed to the formation of clusters with sizes of a few nanometers. The clusters showed no contrast in high resolution TEM images. No β″ phase precipitates were detected.

Fig. 7 shows two-beam bright field images obtained near the $[01\bar{1}]$ matrix zone axis of specimens pre-aged 180 min at RT (a) or at

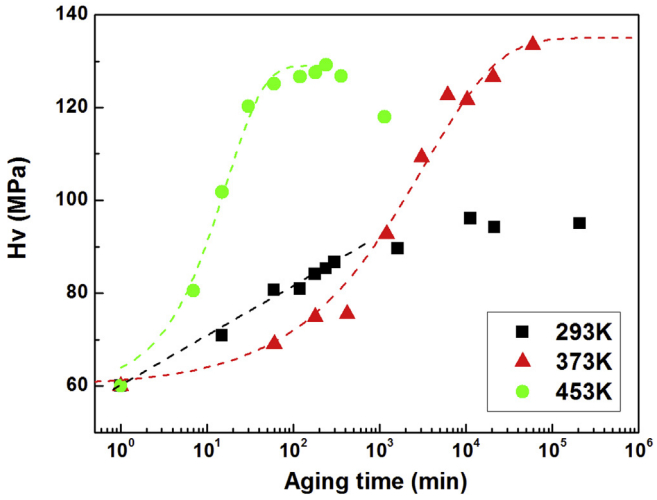

Fig. 4. Hardness evolution during isothermal ageing at 293 K, 373 K and 453 K.

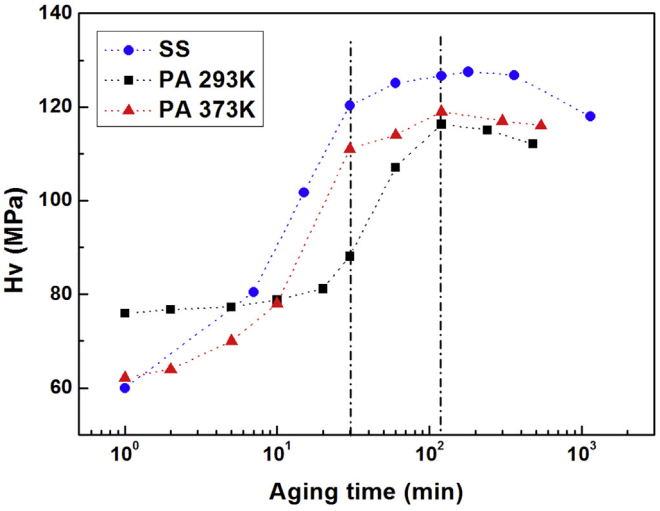

Fig. 5. Hardness evolution during AA at 453 K measured directly after quenching (SS), and following pre-ageing for 180 min at 293 K and 373 K.

373 K (b), and subsequently aged during 30 min at 453 K (marks in Fig. 5). In both specimens the observed contrast corresponds to needle-shaped β″ precipitates oriented parallel to the ⟨100⟩ matrix directions, and whose projections are oriented parallel to the [1 0 0] and the [0 1 1] directions. The density of precipitates is higher and the average size is smaller in the specimen with pre-aging at 373 K that those in the RT pre-aged specimens.

Fig. 8 shows STEM annular bright field (ABF) images along the [001] matrix zone axis (a,b) and High Resolution images (c,d) of specimens with PA at RT (a,c) or 373 K (b,d), subsequently aged at 453 K for 120 min, corresponding to the peak hardness condition (Fig. 5). Three needle-shaped β″ precipitate variants, oriented along the ⟨100⟩ matrix directions, are indicated. In the high resolution images (c, d) only the needle shaped variants parallel to the [001] direction are observed, since very few precipitates of the other variants are found in the very thin regions of the specimen and their contrast is very low due to the high coherence with the matrix. Using the ABF images, the average precipitate lengths were measured, resulting in (20 ± 1) nm and (14 ± 1) nm for the pre-ageing at room temperature and at 373 K, respectively. The average diameter of the precipitates was measured in the high

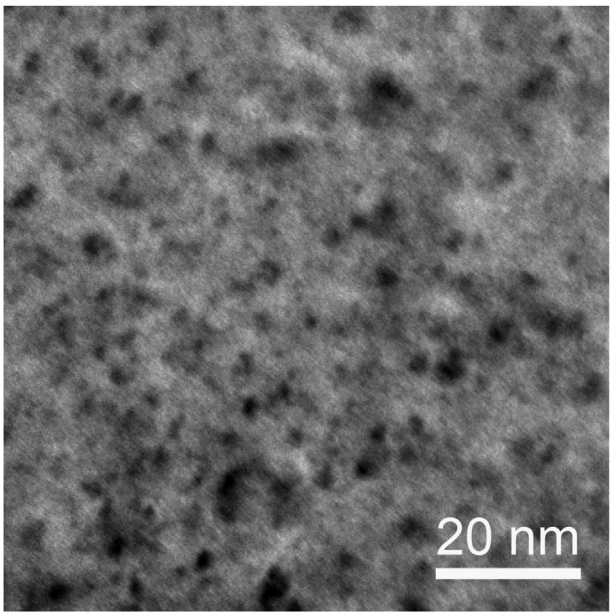

Fig. 6. Bright field image of a specimen aged for 1 week at 373 K.

resolution images. A value of 2.2 nm, for both pre-ageing temperatures was determined.

4. Discussion

The DSC results showed that during pre-ageing different processes occur according to the PA temperature. A “low” temperature behavior and a “high” temperature behavior were identified with a transition temperature around 343 K. These different behaviours can be related to the formation of different types of clusters when pre-ageing is carried out above or below the transition temperature. Those formed below 343 K are named type 1 clusters, while those that form above 343 K are named type 2 clusters.

Different types of clusters according to the pre-ageing temperature have been reported by several authors. For example, Murayama and Hono [14] in alloys with slightly different composition (Al–0.65 wt% Mg–0.7 wt% Si and Al–0.70 wt% Mg–0.55 wt% Si), reported the formation of Mg–Si co-clusters at room temperature, and spherical GP zones at 343 K that had different effects on the microstructural evolution during subsequent artificial ageing at 448 K. Later, Takata et al. [28], reported different types of clusters forming at 363 K and at 323 K in an Al–0.7 wt% Mg–0.7 wt% Si alloy. In both cases, the results presented are consistent with a transition temperature of about 343 K as reported in the present work. Although there is valuable reported information, the clusters composition is still unclear. According to reference [14], from a chemical point of view, clusters formed at low and high aging temperature are essentially the same; the only difference is in the size and the density of solute atoms. Serizawa et al. [16] reported the Mg/Si ratio of approximately 1.5–2.0, reaching a maximum size of around 25 atoms after aging 10^3 day at RT, and of around 175 atoms after 7 days at 373 K. Torsaeter et al. [30] found that nearly all clusters after aging at 373 K are of the Mg1Si1 type, while a significant number of nonbalanced clusters, Si-rich or Mg-rich, were observed after NA. Nonbalanced clusters after prolonged NA were reported also in Refs. [19,33].

In the samples pre-aged at 293 K, type 1 clusters are formed. For PA times of 40 min or more, DSC results show an endothermic signal at around 483 K, which can be attributed to the dissolution of

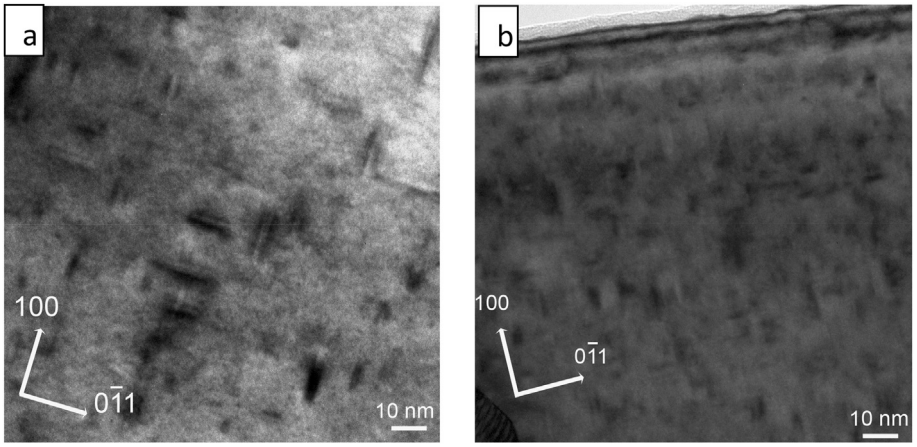

Fig. 7. TEM images corresponding to an AA time of 30 min at 453 K with pre-ageing at RT (a) and at 373 K (b).

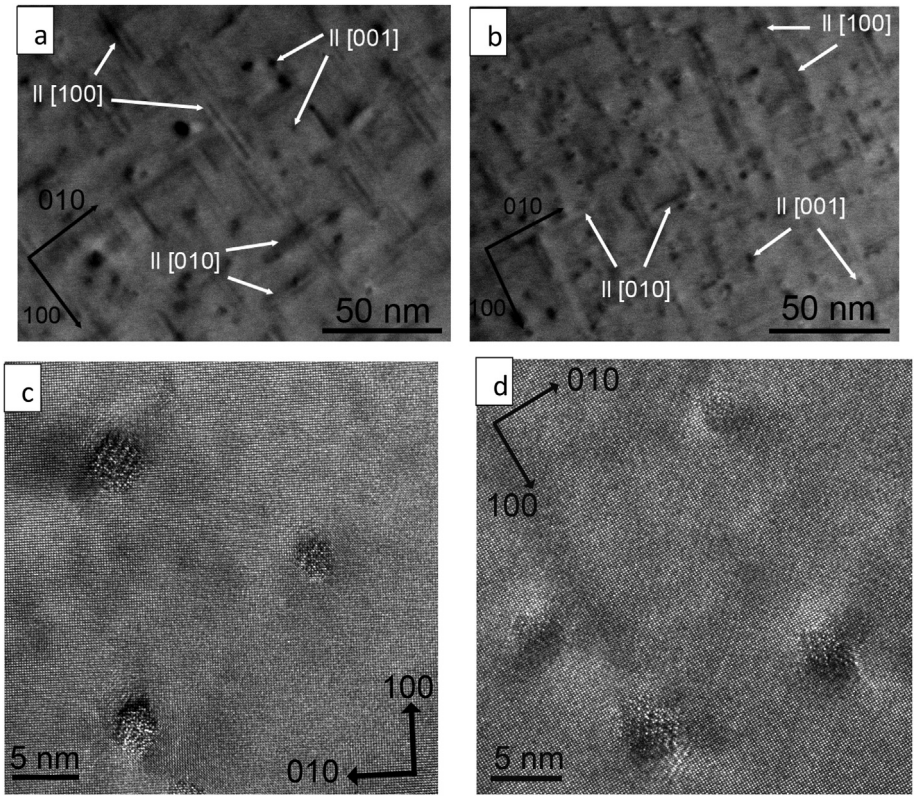

Fig. 8. Annular bright field images (a), (b) obtained in STEM mode and High resolution TEM images (c), (d) of specimens with 180 min PA at RT (a), (c) and at 373 K (b), (d), followed by 120 min AA at 453 K. Zone axis is [001]. The three variants of needle shaper β″ precipitates oriented parallel to the ⟨100⟩ matrix directions are indicated in (a) and (b).

type 1 clusters, prior to the precipitation of the β″ phase. This endothermic peak is more pronounced as the PA time increases, indicating that during PA a progressively higher fraction of Mg and Si atoms form clusters. The observed gradual shift of the β″ phase precipitation peak to higher temperatures with increasing PA time can be explained by the influence of the dissolution of type 1 clusters on such precipitation. Whereas after short PA time the β″ precipitation of the Mg and Si atoms that remain is solid solution (that is, not in type 1 clusters) occurs simultaneously with the dissolution of clusters, for longer PA times the precipitation of the β″ phase is progressively delayed to allow the dissolution of type 1 clusters. Furthermore, the ΔH associated with the nucleation and growth of β″ phase remains constant independently of the PA level, since it measures the enthalpy change between the β″ phase precipitates and the solid solution. The dissolution of clusters 1 at temperatures higher than 483 K has been confirmed by microhardness measurements, with a marked Hv decrease in the first minutes of AA [34].

Contrasting with this behavior, in samples pre-aged at 373 K there is no indication of an endothermic signal, and, as the PA increases, the peak temperature Tp decreases and the ΔH associated with the nucleation and growth of β″ phase is reduced. These effects indicate that the type 2 clusters do not dissolve, but serve, instead, as β″ precipitate nuclei. It has been reported that clusters 2

transform into the β″ phase, and are called pre-β″ by some authors [7,16,30]. The type 2 clusters reported in this work correspond to the GP-zones formed at 343 K in the work of Murayama et al. [14].

The reduction of ΔH as PA time increases indicates that type 2 clusters evolve during PA toward a composition and structure that has a similar formation enthalpy as that of the β″ phase. Therefore, for long PA times, the transformation to the β″ phase occurs with negligible enthalpy change, as presented in the Results section.

Van Huis et al. [13,35] proposed different structures and compositions of type 2 clusters, and calculate their formation enthalpy with respect to the solid solution by first-principles methods. The ΔH difference they obtain between some of those structures and β″ phase is actually small. Phases with Mg:Si ratios higher and lower than 1 are energetically favorable. Some of those with high Al atoms fractions additionally have small lattice mismatch, making them probable candidates for the type 2 clusters. In this case, the transformation of type 2 clusters to β″ would occur with the replacement of Al atoms by Mg and Si atoms [13]. Atom probe tomography studies suggest that the type 2 clusters composition evolves with aging time. It has been reported that after ~10^3 min at 373 K the Mg:Si ratio is close to 1 [30], while in samples aged ~10^5min the Mg:Si ratio approaches the range of 1.5–2 [16].

Analysis of clusters' energy shows that the Mg-enrichment is a condition for clusters stabilization [33]. Simulated compositional evolution suggests that the NA clusters cannot reach the composition required for survival under AA. Our results indicate that type 1 clusters are stable up to around 483 K, and β″ precipitation occurs after or simultaneously with the type 1 clusters dissolution. The relative stability of NA clusters leads to less solute availability for clustering or precipitation under subsequent aging at temperatures below 483 K [7,22,30]. The high Mg/Si ratio reached by clusters under aging at 373 K leads to their relative stabilization, and subsequent transformation to β″ phase [33]. First-principle calculations of formation enthalpies have shown that they monotonically decrease in the order of the observed phase transformation: $\Delta H(SS) \geq \Delta H(\text{pre-}\beta'') \geq \Delta H(\beta'')$ [4]. We found that pre-β″ particles, or type 2 clusters, reach a composition/structure under extended 373 K aging which make $\Delta H(\text{pre-}\beta'') \approx \Delta H(\beta'')$.

Both type of clusters share a high density of Mg and Si atoms. However, they show different hardening behavior. While the evolution of hardness corresponding to type 1 clusters reaches a plateau, that of type 2 clusters continues to grow after long PA times. This effect is another indication of the evolution of type 2 clusters, consistent with the results of reference [16]. Hardening under AA at 453 K shows the three expected stages, underaging, peak aging, and overaging. It is important to notice that long-time aging at 373 K leads to higher hardness than that measured at the peak aging, indicating that the final distribution of type 2 clusters is more effective to hamper dislocation glide compared with that of the β″ needle-shaped precipitates formed at 453 K.

From the hardness evolution, the degree of clustering can be analyzed as a fraction transformed f, proportional to the number of clustered atoms, given by:

$$f = \frac{Hv(t) - Hv_0}{Hv_m - Hv_0} \tag{1}$$

where Hv(t) is the hardness corresponding to ageing time t, and Hv_0 and Hv_m are the hardness values at the beginning and at the end of the transformation [36]. Assuming that both solute and vacancy concentration are the same when the alloy is subjected to the same solution treatment, Torsaeter et al. [28] propose that the formation of the different type of clusters obeys to different mechanisms: local atomic arrangement at RT and long range diffusion at 373 K. In agreement, it has been proposed that type 1 clusters grow by a mechanism of vacancies solute trapping [37]. According to that model atoms are added to clusters following a $n \propto \ln t$ law, with n the number of clustered atoms, and t the RT aging time. Our results of RT aging hardening before the plateau is reached seems to agree with the Zurob et al. model [37], and can be reasonably fitted with a relationship $dHv/d\ln t = (10.8 \pm 0.6)$. Marioara et al. described the hardening due to type 2 clusters with a similar relationship [7]. However, our results do not show a linear increase of Hv with lnt. From 3DAP results it is proposed that RT clustering is not diffusion controlled, as is 373 K clustering [16]. However, measurements begun after 7 days NA, and it is a time at which Hv evolution saturates (Fig. 5). As a consequence it could be the reason by which no type 1 clusters evolution is observed in Ref. [16]. For clusters formed under aging at 373 K up to 10^4 min, Serizawa et al. [16] proposed a clustering kinetics law $n \propto r^3 \propto t^{3/2}$, with r the average radius of clusters. Our results of hardening by type 2 clusters do not show an Hv-$t^{3/2}$ linear relationship, indicating that long range diffusion is limited possibly by mutual impingement. Instead, a nucleation-growth-impigment transformation mechanism is proposed, which can be described with a Johonson, Mehl, Avrami y Kolmogorov (JMAK) equation [38]:

$$f = 1 - e^{-(kt)^n} \tag{2}$$

where n is the Avrami kinetic index, and $k = k_0 e^{-\frac{E}{RT}}$, with E, R, T, k_0 the apparent activation energy, the gas constant, the aging temperature and the preexponential factor, respectively. From Eqs. (1) and (2) an expression for Hv as a function of the aging time can be written as:

$$Hv = Hv_0 + (Hv_m - Hv_0)\left(1 - e^{-(kt)^n}\right) \tag{3}$$

Our results of 373 K aging experimental data where fitted according Eq. (3), with three adjustable parameters, Hv_m, k and n. As shown in Fig. 5 the hardening kinetics can be reasonable described, with $Hv_m = (75 \pm 3)$, $k = (5 \pm 1)10^{-6}$, $n = (0.50 \pm 0.05)$. For comparison, the hardening kinetics due to β″ phase, under ageing at 453 K, was also fitted with Eq. (3), obtaining $Hv_m = (69 \pm 9)$, $k = (1.1 \pm 0.3)10^{-3}$, $n = (1.1 \pm 0.2)$. As can be seen, the kinetic index n for type 2 clusters is almost one half that for β″ precipitation. k is temperature dependent, and cannot be compared.

The TEM results after long ageing at 373 K show a contrast that corresponds to type 2 clusters. This contrast is different from that of β″ precipitates, indicating that the aging temperature is too low for the clusters 2 → β″ phase transformation, supporting previous results presented in Ref. [7].

Microstructural characterization with TEM also indicates that a higher density of smaller sized β″ precipitates is obtained after 30 min AA at 453 K when PA is carried out al 373 K compared to that at RT. A similar effect was also observed after longer AA of 2 h at 453 K. These results illustrate the effect of PA at different temperatures on the precipitation of the β″ phase. On one hand, they indicate that PA at 373 K favors the nucleation of β″ precipitates, confirming that type 2 clusters serve as nuclei for such precipitates. On the other, they support the interpretation of the delay of the hardening kinetics by PA at RT, attributed to the formation of type 1 clusters that must dissolve to allow the formation of β″ precipitates. In this case, nucleation of such precipitates occurs at 453 K, with a smaller undercooling than that at 373 K, and leading to a coarser microstructure.

5. Conclusions

The clusters formed during pre-ageing at temperatures between 293 K and 373 K and their evolution with increasing time were

systematically characterized in a 6082 Aluminum alloy mainly through DSC experiments, complemented with hardness measurements and TEM observations. The main results and conclusions are:

- A pre-aging transition temperature around 343 K was identified, related to the formation of different types of clusters when pre-ageing is carried out below or above that temperature, named type 1 and type 2 clusters, respectively.
- The dissolution of type 1 clusters occurs concurrently with the β″ precipitation, and the enthalpy change associated with the latter precipitation remains almost constant. In contrast, type 2 clusters evolve reaching a structure and composition with formation enthalpy similar to that of β″ phase.
- Hardness increases during NA according a $Hv \propto \ln t$ law, reaching a saturation value after around 10^4 min. Aging up to 5.9 10^4 min at 373 K leads to a continuous Hv increase, which can be described with a JMAK type equation. The kinetic index n is almost one half of that for β″ precipitation. Moreover, long-time aging at 373 K leads to higher hardness than the maximum reached under AA at 453 K.
- TEM observations of a sample aged 10^4 min at 373 K reveal a dotted aspect indicating a high density of type 2 clusters, a few nanometers in size. No β″ phase was detected. The size and density of β″ precipitates after AA at 453 K denote that type 2 clusters favour its nucleation, contrary to clusters 1.

Acknowledgments

This work was supported by CONICET, ANPCYT, SECAT-UNCentro, UNCuyo, and CICPBA, Argentina.

References

[1] I. Dutta, S.M. Allen, A calorimetric study of precipitation in commercial aluminium alloy 6061, J. Mater. Sci. Lett. 10 (1991) 323–326.
[2] I. Polmear, Light Alloys, fourth ed., Butterworth-Heinemann, Amsterdam, 2006.
[3] K. Matsuda, T. Kawabata, Y. Uetani, T. Sato, S. Ikeno, High-resolution elemental maps for three directions of Mg2Si phase in Al-Mg-Si alloy, J. Mater. Sci. 37 (2002) 3369–3375.
[4] C. Ravi, C. Wolverton, First-principles study of crystal structure and stability of Al-Mg-Si-(Cu) precipitates, Acta Mater. 52 (2004) 4213–4227.
[5] S.J. Andersen, H.W. Zandbergen, J. Jansen, C. Traeholt, U. Tundal, O. Reiso, The crystal structure of the β″ phase in Al-Mg-Su alloys, Acta Mater. 46 (1998) 3283–3298.
[6] R. Vissers, M.A. van Huis, J. Jansen, H.W. Zandbergen, C.D. Marioara, S.J. Andersen, The crystal structure of the β′ phase in Al–Mg–Si alloys, Acta Mater. 55 (2007) 3815–3823.
[7] C.D. Marioara, S.J. Andersen, J. Jansen, H.W. Zandbergen, The influence of temperature and storage time at RT on nucleation of the β″ phase in a 6082 Al–Mg–Si alloy, Acta Mater. 51 (2003) 789–796.
[8] G.A. Edwards, K. Stiller, G.L. Dunlop, M.J. Couper, The precipitation sequence in Al–Mg–Si alloys, Acta Mater. 46 (1998) 3893–3904.
[9] L.C. Doan, K. Nakai, Y. Matsuura, S. Kobayashi, Y. Ohmori, Effects of excess Mg and Si on the isothermal ageing behaviours in the Al-Mg2Si alloys, Mat. Trans. 43 (2002) 1371–1380.
[10] D.J. Chakrabarti, D.E. Laughlin, Phase relations and precipitation in Al-Mg-Si alloys with Cu additions, Prog. Mater. Sci. 49 (2004) 389–410.
[11] C.S. Tsao, C.Y. Chen, U.S. Jeng, T.Y. Kuo, Precipitation kinetics and transformation of metastable phases in Al-Mg-Si alloys, Acta Mater. 54 (2006) 4621–4631.
[12] C. Wolverton, Solute-vacancy binding in aluminum, Acta Mater. 55 (2007) 5867–5872.
[13] M.A. van Huis, J.H. Chen, M.H.F. Sluiter, H.W. Zandbergen, Phase stability and structural features of matrix-embedded hardening precipitates in Al–Mg–Si alloys in the early stages of evolution, Acta Mater. 55 (2007) 2183–2199.
[14] M. Murayama, K. Hono, Pre-precipitate clusters and precipitation processes in Al–Mg–Si alloys, Acta Mater. 47 (1999) 1537–1548.
[15] H. Seyedrezai, D. Grebennikov, P. Mascher, H.S. Zurob, Study of the early stages of clustering in Al–Mg–Si alloys using the electrical resistivity measurements, Mater. Sci. Eng. A 525 (2009) 186–191.
[16] A. Serizawa, S. Hirosawa, T. Sato, Three-dimensional atom probe characterization of nanoclusters responsible for multistep aging behavior of an Al-Mg-Si alloy, Met. Mater. Trans. A 39 (2008) 243–251.
[17] T. Abid, A. Boubertakh, S. Hamamda, Effect of pre-aging and maturing on the precipitation hardening of an Al–Mg–Si alloy, J. Alloys Compd. 490 (2010) 166–169.
[18] A. Serizawa, T. Sato, in: J. Hirsch, B. Skrotzki, G. Gottstein (Eds.), Aluminium Alloys, Wiley-VCH, Weinheim, 2008.
[19] M. Murayama, K. Hono, M. Saga, M. Kikuchi, Atom probe studies on the early stages of precipitation in Al–Mg–Si alloys, Mater. Sci. Eng. A 250 (1998) 127–132.
[20] J. Banhart, C. Chang, Z. Liang, N. Wanderka, M.D.H. Lay, A.J. Hill, Natural aging in Al-Mg-Si alloys – a process of unexpected complexity, Adv. Eng. Mater. 12 (2010) 559–571.
[21] L. Cao, P.A. Rometsch, M.J. Couper, Clustering behaviour in an Al–Mg–Si–Cu alloy during natural ageing and subsequent under-ageing, Mater. Sci. Eng. A 559 (2013) 257–261.
[22] A. Cuniberti, A. Tolley, M.V. Castro Riglos, R.Giovachini, Influence of natural aging on the precipitation hardening of an AlMgSi alloy, Mater. Sci. Eng. A 527 (2010) 5307–5311.
[23] S. Esmaeili, X. Wang, D.J. Lloyd, W.J. Poole, On the precipitation-hardening behavior of the Al-Mg-Si-Cu alloy AA6111, Met. Mater. Trans. A 34 (2003) 751–763.
[24] S. Esmaeili, D.J. Lloyd, Effect of composition on clustering reactions in AlMg-Si(Cu) alloys, Scr. Mater. 50 (2004) 155–158.
[25] S. Esmaeili, D.J. Lloyd, Modeling of precipitation hardening in pre-aged AlMgSi(Cu) alloys, Acta Mater. 53 (2005) 5257–5271.
[26] L. Ding, Y. He, Z. Wen, P. Zhao, Z. Jia, Q. Liu, Optimization of the pre-aging treatment for an AA6022 alloy at various temperatures and holding times, J. Alloys Compd. 647 (2015) 238–244.
[27] W.F. Miao, D.E. Laughlin, A differential scanning calorimetry study of aluminum alloy 6111 with different pre-aging treatments, J. Mater. Sci. Lett. 19 (2000) 201–203.
[28] K. Takata, J. Takahashi, M. Saga, K. Ushioda, A. Hibino, M. Kikuchi, Effect of two-step aging on Cluster Formation in Al-Mg-Si alloys, Mat. Trans. 55 (2014) 885–891.
[29] J. Kim, E. Kobayashi, T. Sato, Effects of Cu addition on behavior of nanoclusters during multi-step aging in Al-Mg-Si alloys, Mat. Trans. 52 (2011) 906–913.
[30] M. Torsaeter, H.S. Hasting, W. Lefebvre, C.D. Marioara, J.C. Walmsley, S.J. Andersen, R. Holmestad, The influence of composition and natural aging on clustering during preaging in Al–Mg–Si alloys, J. Appl. Phys. 108 (2010), 073527–1-9.
[31] L.C. Doan, Y. Ohmori, K. Nakai, Precipitation and dissolution reactions in a 6061 aluminum alloy, Mat. Trans. JIM 41 (2000) 300–305.
[32] A. Garber, K. Matsuda, A.M. Ali, Y. Zou, S. Ikeno, DSC and HRTEM investigation of the precipitates in Al–1.0%Mg2 Si–0.5%Ag alloy, Mat. Sci. Tech. 20 (2004) 1627–1631.
[33] V. Fallah, B. Langelier, N.O. Opoku, B. Raeisinia, N. Provatas, S. Esmaeili, Cluster evolution mechanisms during aging in Al-Mg-Si alloys, Acta Mater. (2016) 290–300.
[34] A. Cuniberti, R. Giovachini, Private communication.
[35] M.A. van Huis, J.H. Chen, H.W. Zandbergen, M.H.F. Sluiter, Phase stability and structural relations of nanometer-sized, matrix-embedded precipitate phases in Al–Mg–Si alloys in the late stages of evolution, Acta Mater. 54 (2006) 2945–2955.
[36] E.J. Mittelmeijer, L. Cheng, P.J. van der Schaaf, C.M. Brackman, B.M. Korevaar, Analysis of nonisothermal transformation kinetics; Tempering of Iron-Nirogen martensites, Met. Trans. A 19 (1988) 925–932.
[37] H.S. Zurob, H. Seyedrezai, A model for the growth of solute clusters based on vacancy trapping, Scr. Mater. 61 (2009) 141–144.
[38] D.A. Portery, K.E. Easterling, Phase Transformations in Metals and Alloys, Cap. 5, second ed., Chapman & Hall, 1992.